Quantum simulation of Cooper pairing with photons

Ming-Xia Huo,[1] Changsuk Noh,[1] B. M. Rodríguez-Lara,[1] and Dimitris G. Angelakis[1,2,*]
[1]*Centre for Quantum Technologies, National University of Singapore, 3 Science Drive 2 117543, Singapore*
[2]*Science Department, Technical University of Crete, Chania, Crete GR-73100, Greece*
(Received 11 September 2012; published 31 October 2012)

We propose a scheme to observe the crossover from weakly to strongly bound pairs with stationary polaritons. We first show how stationary light-matter excitations (polaritons) can realize an optically tunable two-component Bose-Hubbard model with repulsive intraspecies interactions and attractive interspecies interactions. We then discuss the feasibility of generating an effective Fermi-Hubbard model of polaritons exhibiting the crossover behavior. The predicted behavior of the system characterized by a crossover from short- to long-range spatial correlations as interactions are tuned can be efficiently observed by measuring correlation functions on the light exiting the waveguide.

DOI: 10.1103/PhysRevA.86.043840 PACS number(s): 42.50.Gy, 71.10.Pm, 74.20.Fg

I. INTRODUCTION

Superconductivity is undoubtedly one of the most fascinating phenomena in condensed matter systems [1–4]. Bardeen-Cooper-Schrieffer (BCS) theory [5,6] provided the first satisfying explanation of the effect by proposing that fermions form long-range pairs (Cooper pairs) under an arbitrarily weak attractive interaction. Cooper pairs are exhibited in the attractive Fermi-Hubbard (FH) model, where the so-called BCS-BEC crossover was shown to occur [7–13]. Due to the remarkable progress in the field of ultracold atoms trapped in optical lattices [14,15], the FH model has recently been realized experimentally [16–18].

On the other hand, by using bosonic mixtures in a one-dimensional (1D) optical lattice under the regime of strong intraspecies repulsion, a realization of an effective FH model has been proposed [19]. This is done by utilizing the well-known mapping of 1D hard-core bosons into free spin-less fermions [20,21]. In this setup, one could not only observe the 1D version of the BCS-BEC crossover, but also a new regime that appears as the interspecies attraction is increased in comparison to the intraspecies repulsion. The system was shown to move away from the fermionic BCS-BEC regime and enter into a new strongly localized bosonic phase, termed "big boson" (BB), where almost all the bosonic molecules occupy the same site [19].

Working along the lines of the two-species-boson model studied by the authors of [19], we introduce a quantum simulator made out of massless photons, instead of massive cold atoms as in previous proposals, to probe the typical crossover physics. In earlier works investigating the crossover using cold atoms, only the density profiles and indirect measurements of the gap are made using time-of-flight measurements. Efficient correlation measurements, which would reveal more information on the effects in question are still challenging to obtain there. Our complementary system, of fundamentally different origin, is able to provide such correlations via standard measurements on optical coherence functions of the emitted photons from the medium. Specifically, our work is motivated by recent progress in the field of photonic quantum simulations using 1D nonlinear waveguides [22–24], where photon crystallization, Luttinger liquids behavior, and the "Pinning transition" have been predicted [25–29]. In this area, it is still not clear how one could engineer the waveguide system doped with four-level atoms to generate two-species of polaritons obeying the Lieb-Liniger dynamics with repulsive intraspecies and attractive interspecies interactions, and whether this system can be driven to the "weak interaction and deep potential" regime, where the crossover occurs.

To answer the above questions, we first introduce the setup and analyze the parameter regime for the generation of a highly tunable two-component Bose-Hubbard (BH) model of polaritons [30–36]. We then investigate the possibility of tuning the polaritonic repulsive intraspecies interactions strong enough to generate effective fermionic behavior. Next the interspecies interactions are tuned to be attractive, allowing for the observations of the (1D version of) BCS-BEC-BB crossover by analyzing the spatial correlations of the trapped excitations. The last of these can be efficiently performed by coherently mapping the polaritons into propagating photons which are then measured as they exit the waveguide.

II. MODEL SETUP

Our proposal exploits strong nonlinearities and wide tunability available in photonic systems based on the electromagnetically induced transparency (EIT) effect. Two experimental candidates in this direction have been proposed recently, where cold atomic ensembles are brought closer to the surface of a tapered fiber [37,38] or are loaded inside the core of a hollow-core waveguide [39–43] as depicted in Fig. 1(a). Two species of cold atoms a and b with linear densities n^a and n^b are considered in our scheme. The procedure to observe the desired phenomena can be summarized into the following steps: preparation of laser-cooled atoms and light fields, generation of stationary polaritons, and the lattice potential, steering the system to a particular regime (phase) and finally releasing the polaritons into outgoing photons to measure characteristic correlations. In the first step, laser-cooled atoms with four hyperfine levels are prepared in the ground states and then transferred into the hollow-core waveguide via cold atoms transferring techniques [41–43] or brought closer to the surface of a nanofiber [37,38]. Two

*dimitris.angelakis@gmail.org

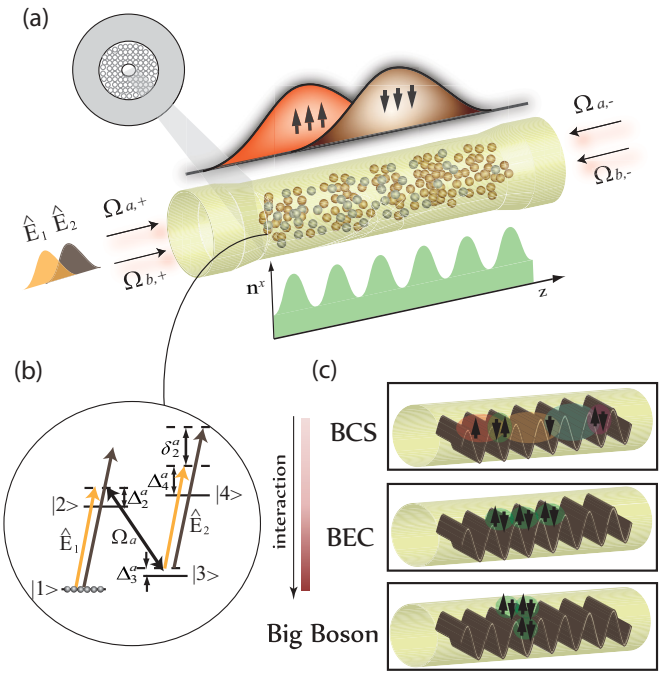

FIG. 1. (Color online) (a) A schematic diagram of the system under study. In a fiber setup (a hollow core version is shown here [43] but a tapered fiber approach [38] could also be used), cold atoms are interacting with a pair of quantum fields $\hat{E}_{1,2}$, and a pair of classical fields $\Omega_{a,b}$. The resulting stationary light-matter excitations in the waveguide can be steered to a strongly interacting regime mimicking an effective FH model with highly tunable attractive interactions. (b) The atomic level structure for a type-a atom. Type-b atoms have similar structure but primarily coupled to $\hat{E}_2$ (c) Schematic illustration of interesting phases discussed in the text. Coherently mapping the stationary excitations to propagating photon pulses allows for the efficient probing of the BCS-BEC crossover by measuring the temporal correlations of the photon pulses leaving the fiber.

right-propagating quantum fields, $\hat{E}_{j,+}(z,t)$ with $j = 1,2$, and two co-propagating classical fields, $\Omega_{x,+}(t)$ with $x = a,b$, are then injected into the waveguide. The two quantum fields then interact with atoms as in the typical EIT-based scheme. Here, the probe beams $\hat{E}_{j,+}(z,t)$ are coherently converted into atomic excitations by adiabatically switching off the control beams $\Omega_{x,+}(t)$ after the quantum pulses $\hat{E}_{j,+}(z,t)$ completely enter the medium. In the second step, the left- and right-propagating control fields $\Omega_{x,-}(t)$ and $\Omega_{x,+}(t)$ are slowly turned on to form two standing wave patterns. The resulting Bragg gratings create stationary excitations [30–35]. Such a (coherent) stationary polaritonic state is the ground state of the system as the initial state of the following process. After tuning the parameters and achieving the desired state, switching off $\Omega_{x,-}(t)$ converts the polaritons into traveling photons, measuring which establishes the density-density correlation functions. Although a numerical analysis is needed to obtain precise answers, during the whole adiabatic operation process the initial state remains in the ground state of the instantaneous Hamiltonian to a good approximation, so that the final state is approximately the ground state of the final Hamiltonian.

At the second stage, the Hamiltonian in the interaction picture reads

$$H = H^a + H^b, \tag{1}$$

with

$$\begin{aligned} H^x = -\hbar n^x \int dz \Big\{ & \Delta_2^x \sigma_{22}^x + \Delta_3^x \sigma_{33}^x + \Delta_4^x \sigma_{44}^x \\ & + \sqrt{2\pi} \sum_{j=1}^{2} g_j^x \left(\sigma_{21}^x + \sigma_{43}^x\right) e^{i\delta_j^x t} \\ & \times \left(\hat{E}_{j,+} e^{ik_{\rm qu}^{(j)} z} + \hat{E}_{j,-} e^{-ik_{\rm qu}^{(j)} z}\right) \\ & + \left[\left(\Omega_{x,+} e^{ik_{\rm cl}^{(x)} z} + \Omega_{x,-} e^{-ik_{\rm cl}^{(x)} z}\right)\sigma_{23}^x + \text{H.c.}\right]\Big\}, \end{aligned} \tag{2}$$

where $x = a,b$. For simplicity, we omit the space and time dependence of the operators. The continuous collective atomic spin operators $\sigma_{pq}^x \equiv \sigma_{pq}^x(z,t)$ give the averages of $|p\rangle^x\langle q|$ over the x-type atoms in a small but macroscopic region around z. The wave numbers and central frequencies of the slowly varying quantum and classical fields are denoted by $k_{\rm qu}^{(1,2)}$, $k_{\rm cl}^{(a,b)}$ and $\omega_{\rm qu}^{(1,2)}$, $\omega_{\rm cl}^{(a,b)}$, and the quantum pulse detunings as $\delta_2^a = \omega_{\rm qu}^{(1)} - \omega_{\rm qu}^{(2)}$, $\delta_1^b = -\delta_2^a$ with $\delta_1^a = \delta_2^b = 0$. g_j^x is the single-photon-single-atom coupling constant between an x-type atom and the jth quantum field. For simplicity $\hat{E}_{(1,2)}$ are assumed to be coupled to the transitions $|2\rangle^x\langle 1|$ and $|4\rangle^x\langle 3|$ with the same strengths $g_{(1,2)}^x$. One-photon detunings are denoted by Δ_2^x and Δ_4^x, and the two-photon detunings are Δ_3^x, where the detunings for $x = a,b$ are defined with respect to the probe fields 1,2, respectively [see Fig. 1(b)].

The evolution of the quantum fields $\hat{E}_{j,\pm}$ in the nonlinear medium is described by the Maxwell-Bloch equations

$$\begin{aligned} & (\partial_t \pm v_j \partial_z)\hat{E}_{j,\pm} \\ & = -i v_j \Delta\omega_j \hat{E}_{j,\pm} + i\sqrt{2\pi} n^{x_j} g_j^{x_j} \\ & \quad \times \left[\sigma_{12,\pm}^{x_j}(z,t) + \sigma_{34,\pm}^{x_j}(z,t)\right] + i\sqrt{2\pi} n^{\bar{x}_j} g_j^{\bar{x}_j} \\ & \quad \times \left[\sigma_{12,\pm}^{\bar{x}_j}(z,t) + \sigma_{34,\pm}^{\bar{x}_j}(z,t)\right] e^{\mp i\delta_1^b} e^{\pm(k_{\rm qu}^{(2)} - k_{\rm qu}^{(1)})}, \end{aligned} \tag{3}$$

where $j = 1,2$, $x_1 = a$, $x_2 = b$, and $\bar{x}_1 = b$, $\bar{x}_2 = a$. Here the slowly varying collective atomic operators $\sigma_{pq}^{x_j}(z,t) = e^{ik_{\rm cl}^{(x_j)}} \sigma_{pq,+}^{x_j}(z,t) + e^{-ik_{\rm cl}^{(x_j)}} \sigma_{pq,-}^{x_j}(z,t)$ have been introduced. $v_j = \omega_{\rm qu}^{(x_j)}/k_{\rm qu}^{(j)}$ is the speed of the quantum fields $\hat{E}_{j,\pm}$ in an empty waveguide and $\Delta\omega_j = \omega_{\rm cl}^{(x_j)} - \omega_{\rm qu}^{(j)}$ is the frequency difference between the classical and quantum fields. The collective atomic operators obey the usual Langevin-Bloch equations that can be solved following the standard method in the literature [34,44,45]. After adiabatic elimination of the fast-decaying operators, slowly varying operators can be solved in terms of the right- and left-propagating polariton operators $\Psi_{j,\pm} = g_j^{x_j}\sqrt{2\pi n^{x_j}}\hat{E}_{j,\pm}/\Omega_{x_j}$ that describe the long-lived stationary light-matter excitations of the system. Note that we have assumed $\Omega_{x_j} = \Omega_{x_j,\pm}$. Substituting the result into the Maxwell-Bloch equations, we find that the stationary polariton operators $\Psi_j = (\Psi_{j,+} + \Psi_{j,-})/2$ obey two coupled

nonlinear Schrödinger equations [25–29]

$$i\partial_t \Psi_j = -\frac{1}{2m_j}\nabla^2\Psi_j + V_j\Psi_j + 2\chi_j\Psi_j^\dagger\Psi_j^2 + \chi_{12}\Psi_j\Psi_{\bar{j}}^\dagger\Psi_{\bar{j}} \tag{4}$$

with $\bar{j} \neq j$. This equation can be derived from a two-component Lieb-Liniger (LL) Hamiltonian

$$H = \int dz \sum_{j=1}^{2}\left\{\Psi_j^\dagger\left[\frac{1}{2m_j}\nabla^2 + V_j\right]\Psi_j + \chi_j\Psi_j^\dagger\Psi_j^\dagger\Psi_j\Psi_j\right\} + \chi_{12}\int dz\Psi_1^\dagger\Psi_1\Psi_2^\dagger\Psi_2. \tag{5}$$

The one-photon detunings Δ_2^x lead to a quadratic dispersion of the polaritons where the effective polaritonic masses are

$$m_j = -\frac{\Gamma_j^{1D} n^{x_j}}{4\Delta_2^{x_j} v_j^g}. \tag{6}$$

Here, $v_j^g = v_j\Omega_{x_j}^2/(\pi g^2 n^{x_j})$ is the group velocity of j-type polaritons in the nonlinear medium where we have assumed that $g_j^{x_j} = g$ for simplicity. $\Gamma_j^{1D} = 4\pi g^2/v_j$ is the spontaneous emission rate of a single x_j-type atom into the waveguide modes. The second term in Eq. (5) gives an effective potential

$$V_j = \frac{\Delta\omega_j v_j^g}{v_j} - \frac{\Lambda^{x_j}\Gamma_j^{1D}\Delta_3^{x_j} v_j^g n^{x_j}}{4\Omega_{x_j}^2}. \tag{7}$$

Normally, this term is reduced to zero by tuning $\Delta\omega_j$, but in this work we will utilize this term to produce a lattice potential as shown below. The nonlinear terms corresponding to intraspecies and interspecies interactions are given by

$$\chi_j = \frac{(\Lambda^{x_j})^2\Xi^{x_j}\Gamma_j^{1D} v_j^g}{2\Delta_4^{x_j}} \tag{8}$$

and

$$\chi_{12} = \frac{n^a(\Lambda^a\Omega_b)^2\Xi^a\Gamma_1^{1D}v_1^g}{n^b\Omega_a^2\left(\Delta_4^a - \delta_2^a\right)} + \frac{n^b(\Lambda^b\Omega_a)^2\Xi^b\Gamma_2^{1D}v_2^g}{n^a\Omega_b^2\left(\Delta_4^b - \delta_1^b\right)}, \tag{9}$$

where two dimensionless quantities $\Lambda^x = \Omega_x^2/(\Omega_x^2 - \Delta_3^x\Delta_2^x/2)$ and $\Xi^x = (\Delta_4^x - \Delta_3^x/2)/(\Delta_4^x - \Delta_3^x)$ are introduced. As one would expect, the above nonlinear terms are inversely proportional to the single photon detunings of the quantum fields with respect to the transitions $|3\rangle^x \leftrightarrow |4\rangle^x$.

To add effective polaritonic lattices commensurate to each of the photonic densities n_j^{ph}, we follow the method outlined in [28] for single species of photons. By applying standing microwave fields, some atoms are transferred from the ground state $|1\rangle^x$ to an irrelevant state $|u\rangle^x$, thus creating slightly modulated atomic densities in the ground state $|1\rangle^x$

$$n^{x_j} = n_0^{x_j} + n_1^{x_j}\cos^2\left(\pi n_j^{ph} z\right), \tag{10}$$

where we have assumed that $n_0^{x_j} \gg n_1^{x_j}$. For standing microwave fields, the transfer rate p_u^x from $|1\rangle^x$ to $|u\rangle^x$ is $(\Omega_{M.W.}^x)^2\cos^2(\pi n_j^{ph} z)t^2$ [46]. Switching on two microwave fields for $t \sim 6$ ns transfers ten percent of atoms from $|1\rangle^x$ to $|u\rangle^x$, corresponding to $n_1^{x_j} \simeq 0.1 n^{x_j}$. For $n_j^{ph} = 300\,\mathrm{m}^{-1}$, the wavelengths of the microwave fields should be 2–3 cm, which indicates that the frequency difference between states $|1\rangle^x$ and $|u\rangle^x$ should be around 45 GHz. With the modulation, the potentials V_j become

$$V_j = \frac{\Delta\omega v_j^g}{v_j} - \frac{\Lambda^{x_j}\Gamma_j^{1D}\Delta_3^{x_j} v_j^g n_0^{x_j}}{4\Omega_{x_j}^2} - \frac{\Lambda^{x_j}\Gamma_j^{1D}\Delta_3^{x_j} v_j^g n_1^{x_j}\cos^2\left(\pi n_j^{ph} z\right)}{4\Omega_{x_j}^2}. \tag{11}$$

Choosing $\Delta\omega = \Lambda^{x_j}\Gamma_j^{1D}\Delta_3^{x_j} v_j n_0^{x_j}/(4\Omega_{x_j}^2)$, the effective potentials reduce to $V_j = \mu_j\cos^2(\pi n_j^{ph} z)$ with lattice depths

$$\mu_j = -\frac{\Lambda^{x_j}\Gamma_j^{1D}\Delta_3^{x_j} v_j^g n_1^{x_j}}{4\Omega_{x_j}^2}. \tag{12}$$

For simplicity, we assume the symmetric situation where all the species-dependent parameters are identical: $\Omega_x = \Omega$, $n_j^{ph} = n^{ph}, n^x = n, n_1^x = n_1, v_j = v, v_j^g = v^g, \Gamma_j^{1D} = \Gamma^{1D}$, and $\Delta_k^x = \Delta_k$ for $k = 2,3,4$. The interaction parameters thus lose their subscript j in the following.

III. DECOHERENCE

We first recall that the parameters in the coupled nonlinear Schrödinger equations, Eq. (4), have nonzero imaginary parts that describe photon losses [25]. These as we show can be ignored in the limit of large single photon detunings and as long as the evolution time does not exceed the coherence time defined by the total loss rate. We show that both conditions are satisfied in our setup. Including photon losses the parameters read

$$m = -\frac{\Gamma^{1D} n}{4(\Delta_2 + i\Gamma)v^g}, \tag{13}$$

$$\chi \simeq \frac{\Gamma^{1D} v^g}{2(\Delta_4 + i\Gamma)}, \tag{14}$$

$$\chi_{12} \simeq \frac{2\Gamma^{1D} v^g(\Delta_4 + i\Gamma)}{(\Delta_4 + i\Gamma)^2 - \left(\delta_1^b\right)^2}. \tag{15}$$

The potential V also has a nonzero imaginary component, but the loss term is negligible compared to other terms. The linear loss term, which results from a finite bandwidth of the EIT transparency window, can be written as

$$\frac{\partial\Psi_j}{\partial t} \sim \frac{v^g\Gamma}{n\Gamma^{1D}}\frac{\partial^2\Psi_j}{\partial z^2}. \tag{16}$$

The loss terms coming from the nonlinear intraspecies and interspecies interactions are given by

$$\frac{\partial\Psi_j}{\partial t} \sim \frac{1}{2}\frac{\Gamma^{1D}\Gamma v^g\Psi_j^\dagger\Psi_j^2}{\Delta_4^2}, \tag{17}$$

$$\frac{\partial\Psi_j}{\partial t} \sim 2\frac{\Gamma^{1D}\Gamma\left[\Delta_4^2 + \left(\delta_1^b\right)^2 + \Gamma^2\right]v^g\Psi_j\Psi_{\bar{j}}^\dagger\Psi_{\bar{j}}}{\left[(\Delta_4)^2 - \left(\delta_1^b\right)^2\right]\left[\Delta_4^2 - \left(\delta_1^b\right)^2 + \Gamma^2\right]}. \tag{18}$$

In the strong coupling regime, the largest spatial components are given by $\Delta z \sim (n^{ph})^{-1}$, where n^{ph} is the polaritonic

density. Then the loss rates are given by

$$\kappa_1 = \frac{(n^{\rm ph})^2 v^g \Gamma}{n\Gamma^{1D}}, \tag{19}$$

$$\kappa_{\rm ns} = \frac{1}{2}\frac{\Gamma^{1D}\Gamma v^g n^{\rm ph}}{\Delta_4^2}, \tag{20}$$

$$\kappa_{\rm nd} = 2\frac{\Gamma^{1D}\Gamma\left[\Delta_4^2 + \left(\delta_1^b\right)^2 + \Gamma^2\right]v^g n^{\rm ph}}{\left[(\Delta_4)^2 - \left(\delta_1^b\right)^2\right]\left[\Delta_4^2 - \left(\delta_1^b\right)^2 + \Gamma^2\right]}. \tag{21}$$

κ_1 denotes the linear loss rate and $\kappa_{\rm ns}$, $\kappa_{\rm nd}$ denote the nonlinear loss rates coming from intraspecies and interspecies interactions.

For the parameters given in Fig. 2 (i.e., $n/n^{\rm ph} = 10^4$, $n^{\rm ph} = 300\,{\rm m}^{-1}$, $\Gamma \simeq 20\,{\rm MHz}$, $\eta = \Gamma^{1D}/\Gamma = 0.2$, $v^g \sim 100\,{\rm m/s}$, $\Delta_2 = -5\Gamma$, $\Delta_3 = -0.01\Gamma$, $15\Gamma \leqslant \Delta_4 \leqslant 30\Gamma$, and $1.5\Delta_4 \leqslant \delta_1^b \leqslant 5.5\Delta_4$), the maximum total loss rate $\kappa_{\rm total} = \kappa_1 + \kappa_{\rm ns} + \kappa_{\rm nd}$ is 140 Hz, giving the decoherence time of 7 milliseconds. We note that this is long enough to allow for the entire processes of preparation, evolution, and readout.

IV. TWO-COMPONENT POLARITONIC BH AND EFFECTIVE FH MODELS

To map the LL Hamiltonian (5) to a two-species BH model, we assume the control lasers during the second step are ramped up to $\Omega \simeq \Gamma$, and the detunings are set to the values $\Delta_2 = -5\Gamma$, $\Delta_3 = -0.01\Gamma$ (see Fig. 2). As shown in [28] for a single species, when the external microwave fields are slowly turned on to make n_1/n larger than 0.05, the lattices are sufficiently deep to map the LL Hamiltonian (5) to a two-species BH model

$$H = -\sum_{\langle i,j\rangle,\sigma} t_\sigma a_{i\sigma}^\dagger a_{j\sigma} + \sum_{i,\sigma} U_\sigma n_{i\sigma}^2 + V\sum_i n_{i\uparrow}n_{i\downarrow}, \tag{22}$$

where $a_{i\sigma}$ is the annihilation operator of a σ-type polariton at the ith site and $\langle i,j\rangle$ stands for nearest neighbors. The hopping and coupling strengths are given as

$$t_\sigma = \frac{4}{\sqrt{\pi}}\mu^{3/4}E_R^{1/4}\exp(-2\sqrt{\mu/E_R}), \tag{23}$$

$$U_\sigma = \frac{\sqrt{2\pi}}{2}\chi n^{\rm ph}(\mu/E_R)^{1/4}, \tag{24}$$

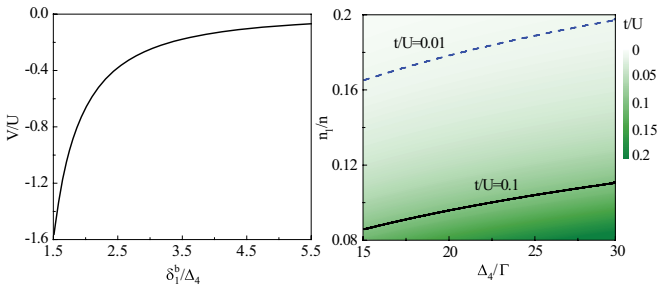

FIG. 2. (Color online) Achievable polaritonic (a) interspecies interaction V/U and (b) hopping strength t/U as functions of the quantum pulse frequency difference δ_1^b, single photon detuning Δ_4, and the atomic distribution modulation n_1/n. Here the parameters are set as $\Gamma_{1D} = 0.2\Gamma$, $n/n^{\rm ph} = 10^4$, $\Delta_2 = -5\Gamma$, $\Omega = \Gamma$, and $\Delta_3 = -0.01\Gamma$.

and

$$V = \frac{\sqrt{2\pi}}{2}\chi_{12}n^{\rm ph}(\mu/E_R)^{1/4}, \tag{25}$$

where $E_R = \pi^2(n^{\rm ph})^2/(2m)$ is the recoil energy. As $t_\uparrow = t_\downarrow$ and $U_\uparrow = U_\downarrow$, we drop their subscripts in the following.

Based on the above expressions, the ratios of interspecies to intraspecies interaction

$$\frac{V}{U} = \frac{2\Delta_4^2}{\Delta_4^2 - \left(\delta_1^b\right)^2}, \tag{26}$$

and the hopping to repulsion

$$\frac{t}{U} = \frac{4\mu^{1/2}E_R^{1/2}\exp(-2\sqrt{\mu/E_R})}{\sqrt{2}\pi\chi n^{\rm ph}} \tag{27}$$

are plotted in Fig. 2. We have chosen the atomic and photonic densities to give $n/n^{\rm ph} = 10^4$ and the single atom cooperativity as $\eta = \Gamma^{1D}/\Gamma = 0.2$ with the typical atomic decay rate for the Rb transition given by $\Gamma \simeq 20\,{\rm MHz}$. These correspond to optical depths of roughly 1000.

The two-component polaritonic BH model described by the Hamiltonian (22) can be mapped to an effective FH model exhibiting the (1D version of) fermion-like BCS-BEC crossover by tuning $t/U \ll 1 - |V|/U$ with $U > 0$ and $V < 0$, where the strong intraspecies repulsion U enforces an effective Pauli exclusion principle. The validity of boson-fermion mapping has been discussed in detail in [19] and although one-body correlations always show bosonic behaviors, density-related observables give the same results for fermions and hard-core bosons. The necessary regime for the mapping can be achieved in our case by setting $\chi > 0$ and $\chi_{12} < 0$ which, assuming $m > 0$, means setting the detunings $\Delta_2 < 0$ and $0 < \Delta_4 < \delta_1^b$. The ratio $t/U \ll 1 - |V|/U$ can be tuned by controlling Δ_4 and n_1/n as shown in Fig. 2, where t/U can be as small as 0.01 while keeping the tunability range of $|V|/U$ relatively large. Beyond this fermion-like limit, when the ratio $|V|/U$ becomes larger, the highly bosonic BB behavior is expected to appear [19]. We would like to point out that different regimes leading to effects such as spin-charge separation or Kondo physics are also accessible.

V. CROSSOVER WITNESS

In BCS- and BEC-like phases, the polaritons form extended Cooper-pair-like objects and localized bosonic molecules, respectively. The correlations which are directly related to these different pairing phenomena can be straightforwardly observed in our system by switching off either the two left- or right-propagating classical fields, hence coherently mapping the stationary polaritonic correlations into propagating photons in the usual slow-light manner [30–35].

In Fig. 3, we calculate the second-order cross-species density-density correlation, $g_{\uparrow\downarrow}^{(2)}(l) = \sum_i \langle n_{i\uparrow}n_{i+l\downarrow}\rangle$, and the density-density correlation between cross-species population differences, $g_-^{(2)}(l) = \sum_i \langle (n_{i\uparrow} - n_{i\downarrow})(n_{i+l\uparrow} - n_{i+l\downarrow})\rangle$, as functions of V/U for the same ($l = 0$), and neighboring ($l = 1$) sites, for two different values of hopping strengths. These correlations can be measured by collecting the component-resolved photon-counting records and analyzing the collected

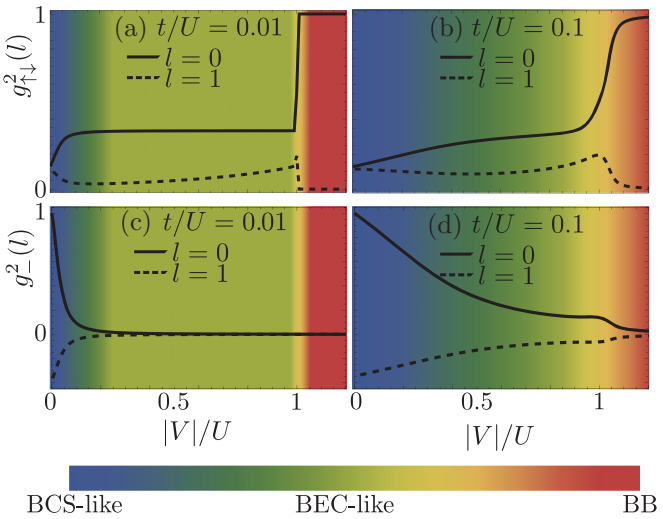

FIG. 3. (Color online) Correlation functions for polaritons: In (a) and (b) the second-order cross-species correlations $g^{(2)}_{\uparrow\downarrow}(l)$ are plotted as functions of the interspecies interaction for the same site ($l = 0$) and neighboring sites ($l = 1$), for two values of hopping strengths $t = 0.01$ and $t = 0.1$. The colored gradient background, proportionate to the on-site cross-species correlation, portrays the BCS-BEC-BB crossover. (c,d) show the correlation between the difference in populations for the two species. Note the sensitivity to the BCS-like phase. The coherent transfer of the polaritonic correlations to propagating photonic ones allows for witnessing the different phases of the system using photon coherence measurements and energy resolving photodetectors.

data. For example, one could use a beam splitter and energy-resolving photon detectors to collect the required data, or one could even make the two species travel in different directions in principle.

More specifically, we numerically compute for illustration (and as a guide for a possible experimental implementation) the ground state of the Hamiltonian (22) for six polaritons in eight sites (i.e., three photons in each quantum pulse and a polaritonic potential modulation with the wave vector $k_m = 2\pi * 8/L$). Here L is the waveguide length taken to be a few centimeters.

The signatures of the BCS-BEC-BB crossover is apparent from the on-site correlation $g^{(2)}_{\uparrow\downarrow}(0)$ as shown in Figs. 3(a) and 3(b). Abrupt changes in $g^{(2)}_{\uparrow\downarrow}(0)$ (normalized to the value at $|V|/U = 1.5$) at $|V| = U$ indicate a transition from the BB state, where all the polaritons pair up at a single site, to the localized pairing (BEC) state, where different pairs prefer to space out. The curves also indicate a crossover from the locally paired (BEC) state (when $|V| \gg t$) to the long-range paired (BCS) state ($|V| \ll t$) which takes place in the Fermionic regime. The colored background portrays the different phases and how they cross over. The black dashed curves show the correlations at $l = 1$, indicating that the photonic BEC pairs space out in the BEC region as $t/|V|$ is increased until the system crosses over to the BCS regime. Figures 3(c) and 3(d) illustrate $g^2_{(-)}(0)$ and $g^2_{(-)}(1)$, respectively, normalized to their values at $|V|/U \to 0$. These show high sensitivity to the BCS-BEC crossover (left side of the subfigures), but are not suitable for observing the BB-BEC crossover. In the photon correlation

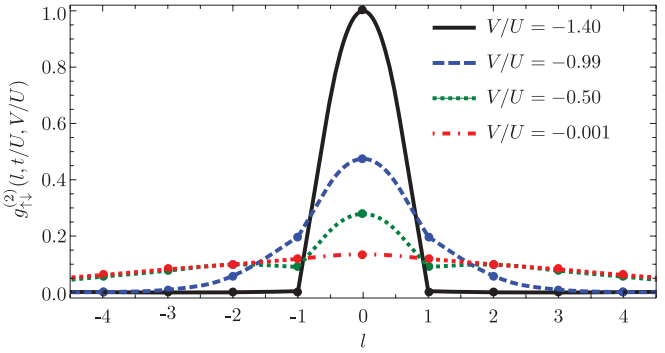

FIG. 4. (Color online) Cross-species second-order correlation function for $t/U = 0.01$ and different values of $|V|/U = 1.4, 0.99, 0.5, 0.001$ as a function of the distance l in units of the effective photonic lattice spacing.

measurements of $g^{(2)}_{\uparrow\downarrow}(0)$, the BCS-BEC-BB crossover appears as a transition from a strongly antibunched behavior in the BCS regime to a highly bunched behavior in the BB regime.

While the correlation functions at $l = 0, 1$ give good signposts for the three phases we have discussed, correlations at longer distances need to be considered, especially in the BCS regime, to completely describe the physics. Figure 4 shows $g^{(2)}_{\uparrow\downarrow}(l)$ for different values of $|V|/U$ with $t/U = 0.01$ fixed as a function of the distance. The expected short-range to long-range correlations are clearly visible in the expected regimes which can also be related to the size of the effective pairs in each case.

VI. CONCLUSION

In conclusion, we have shown that slow-light-EIT-based techniques can be used to controllably prepare and observe strongly correlated states of photons, which makes the realization of two-species polaritonic BH, and thereby effective FH models, possible. The wide tunability of parameters such as interaction strengths and lattice depths allows the BCS-, BEC-like, and BB regimes to be achieved in our photonic system, where, counterintuitively, the physics of massive fermions are simulated using massless photons. After achieving a desired phase, the polaritons are released as outgoing photons for read-out by turning off the classical lasers traveling along one direction. The density-density correlations can provide extremely interesting information on the BCS, BEC, and BB phases of the system, but they are still challenging to obtain in other BCS-BEC-BB crossover proposals. In our system, however, they can be readily measured through the density-density coherence functions of emitted photons using energy resolving photodetectors. The experimental accessibility of correlation functions also makes our scheme an excellent candidate for efficient observations of other fermionic effects such as the Kondo effect and spin-charge separations.

ACKNOWLEDGMENTS

We acknowledge the financial support by the National Research Foundation and Ministry of Education, Singapore.

[1] A. J. Leggett, Nat. Phys. **2**, 134 (2006).
[2] J. Zaanen *et al.*, Nat. Phys. **2**, 138 (2006).
[3] M. Gaudin, Phys. Lett. A **24**, 55 (1967).
[4] C. N. Yang, Phys. Rev. Lett. **19**, 1312 (1967).
[5] J. Bardeen, L. N. Cooper, and J. R. Schrieffer, Phys. Rev. **108**, 1175 (1957).
[6] M. R. Schafroth, Phys. Rev. **96**, 1442 (1954).
[7] P. Nozieres and S. Schmitt-Rink, J. Low Temp. Phys. **59**, 195 (1985).
[8] K. Tanaka and F. Marsiglio, Phys. Rev. B **60**, 3508 (1999).
[9] J. Kinnunen, M. Rodrígues, and P. Törmä, Science **305**, 1131 (2004).
[10] Y. Liao *et al.*, Nature (London) **467**, 567 (2010).
[11] J. N. Fuchs, A. Recati, and W. Zwerger, Phys. Rev. Lett. **93**, 090408 (2004).
[12] I. V. Tokatly, Phys. Rev. Lett. **93**, 090405 (2004).
[13] T. Iida and M. Wadati, J. Phys. Soc. Jpn. **74**, 1724 (2005).
[14] I. Bloch, J. Dalibard, and W. Zwerger, Rev. Mod. Phys. **80**, 885 (2008).
[15] M. Lewenstein *et al.*, Adv. Phys. **56**, 243 (2007).
[16] R. Jördens *et al.*, Nature (London) **455**, 204 (2008).
[17] U. Schneider *et al.*, Science **322**, 1520 (2008).
[18] T. Esslinger, Ann. Rev. Cond. Mat. Phys. **1**, 129 (2010).
[19] B. Paredes and J. I. Cirac, Phys. Rev. Lett. **90**, 150402 (2003).
[20] M. Girardeau, J. Math. Phys. **1**, 516 (1960).
[21] T. Giamarchi, *Quantum Physics in One Dimension* (Oxford University Press, Oxford, 2004).
[22] M. J. Hartmann, F. G. S. L. Brandão, and M. B. Plenio, Nat. Phys. **2**, 849 (2006).
[23] D. G. Angelakis, M. F. Santos, and S. Bose, Phys. Rev. A **76**, 031805(R) (2007).
[24] A. D. Greentree, C. Tahan, J. H. Cole, and L. C. L. Hollenberg, Nat. Phys. **2**, 856 (2006).
[25] D. E. Chang *et al.*, Nat. Phys. **4**, 884 (2008).
[26] D. G. Angelakis, M.-X. Huo, E. Kyoseva, and L. C. Kwek, Phys. Rev. Lett. **106**, 153601 (2011).
[27] E. Shahmoon, G. Kurizki, M. Fleischhauer, and D. Petrosyan, Phys. Rev. A **83**, 033806 (2011).
[28] M.-X. Huo and D. G. Angelakis, Phys. Rev. A **85**, 023821 (2012).
[29] M. Hafezi, D. E. Chang, V. Gritsev, E. A. Demler, and M. D. Lukin, Europhys. Lett. **94**, 54006 (2011).
[30] M. D. Lukin, Rev. Mod. Phys. **75**, 457 (2003).
[31] R. G. Unanyan, J. Otterbach, M. Fleischhauer, J. Ruseckas, V. Kudriasov, and G. Juzeliunas, Phys. Rev. Lett. **105**, 173603 (2010).
[32] J. Otterbach, J. Ruseckas, R. G. Unanyan, G. Juzeliunas, and M. Fleischhauer, Phys. Rev. Lett. **104**, 033903 (2010).
[33] J. Otterbach, R. G. Unanyan, and M. Fleischhauer, Phys. Rev. Lett. **102**, 063602 (2009).
[34] M. Bajcsy, A. S. Zibrov, and M. D. Lukin, Nature (London) **426**, 638 (2003).
[35] M. Bajcsy, S. Hofferberth, V. Balic, T. Peyronel, M. Hafezi, A. S. Zibrov, V. Vuletic, and M. D. Lukin, Phys. Rev. Lett. **102**, 203902 (2009).
[36] M. J. Hartmann, F. G. S. L. Brandão, and M. B. Plenio, New J. Phys. **10**, 033011 (2008).
[37] K. P. Nayak *et al.*, Opt. Express **15**, 5431 (2007).
[38] E. Vetsch, D. Reitz, G. Sague, R. Schmidt, S. T. Dawkins, and A. Rauschenbeutel, Phys. Rev. Lett. **104**, 203603 (2010).
[39] S. Ghosh, J. E. Sharping, D. G. Ouzounov, and A. L. Gaeta, Phys. Rev. Lett. **94**, 093902 (2005).
[40] T. Takekoshi and R. J. Knize, Phys. Rev. Lett. **98**, 210404 (2007).
[41] C. A. Christensen, S. Will, M. Saba, G. B. Jo, Y. I. Shin, W. Ketterle, and D. Pritchard, Phys. Rev. A **78**, 033429 (2008).
[42] S. Vorrath, S. A. Möller, P. Windpassinger, K. Bongs, and K. Sengstock, New J. Phys. **12**, 123015 (2010).
[43] M. Bajcsy, S. Hofferberth, T. Peyronel, V. Balic, Q. Liang, A. S. Zibrov, V. Vuletic, and M. D. Lukin, Phys. Rev. A **83**, 063830 (2011).
[44] M. Fleischhauer and M. D. Lukin, Phys. Rev. Lett. **84**, 5094 (2000).
[45] A. André, M. Bajcsy, A. S. Zibrov, and M. D. Lukin, Phys. Rev. Lett. **94**, 063902 (2005).
[46] C. J. Foot, *Atomic Physics* (Oxford University Press, Oxford, 2005).